A Discrete Oscillator Phase Noise Effect Applied within Phase-Shift Keying RF Digital Signal Modulation

Ricardo J. Simeoni
School of Allied Health Sciences
Griffith University
Gold Coast, Australia
r.simeoni@griffith.edu.au

***Abstract*—This paper presents a simple digital signal modulation/demodulation technique for the purpose of radiofrequency (RF) communications that involves the control of smooth phase amplitude oscillations within a carrier signal. The technique falls under the category of phase-shift keying (PSK) yet is distinctly different from existing PSK techniques. Identification of digital states is achieved via discernment between discrete combinations of off-centre side-lobes about the primary line profile of the carrier spectrum (ala discrete oscillator phase noise), with side-lobes being a function of the above phase amplitude oscillation. For a 2.4 GHz carrier signal, technique variants theoretically allow for competitive data transmission rates of 3 to 8 Mbit/s, which are extendable with variant expansion. Technique robustness (in relation to cryptographic security and resilience towards interference and distortion) is a consequence of amplitude fluctuation immunity, self-referencing at demodulation, smooth waveform transitions between states, single RF source control, and highly distinguishable output states for modest changes in the relevant phase-based modulation parameter.**

Keywords—bluetooth; cryptography; phase shift keying; oscillator phase noise; RF modulation

I. INTRODUCTION

A. Phase-Shift Keying Modulation

A known digital modulation scheme for radiofrequency (RF) communications is that of phase-shift keying (PSK), whereby an RF carrier wave is phase modulated to series transmit digital information. The simplest, and most robust in terms of interference/noise and distortion invulnerability, form of this type of modulation is that of binary phase-shift keying (BPSK) which discretely modulates the phase by 180^o to represent a binary 0 or 1 upon signal demodulation. Because of the just-stated advantages, BPSK only requires relatively low-cost, passive transmitters and has been widely utilized within radiofrequency identification (RFID) business applications. Example business applications within the areas of routine biometric and financial information transfer include passport processing and non-contact pay-wave-type methods of express credit card transactions [1]-[4] (these PSK references apply throughout this Subsection).

Several other PSK variants exist that are more sophisticated or efficient than BPSK. Two such examples (other examples are introduced throughout the paper) include: quadrature phase-shift keying (QPSK) with a comparatively superior bit transmission rate due to a discrete phase modulation between four values, progressively separated by 90^o, to represent one of four 2-bit digital states (binary numbers); and differential binary phase-shift keying (DBFSK) which is a self referencing scheme that is easier to practically implement than BPSK since self-referencing approaches do not require the original carrier signal for comparison at demodulation.

While effective in their application, a disadvantage of PSK variants is that an abrupt (deleterious) amplitude change may accompany a carrier signal's phase change. Furthermore, such abrupt changes can be exacerbated during the low-pass filtering commonly employed by an RF transmitter, and may also be accompanied by as a loss of power from the signal's ideal line frequency spectrum to symmetrical spectral side-lobes about the otherwise ideal line. Some PSK variants to varying degrees reduce the dynamic range of signal amplitude fluctuations via strategies designed to minimize the phase change magnitude of transition pathways on a variant's constellation diagram, which displays binary number representation as a function of phase angle on a two-dimensional polar (longitudinal-type) plot. For example, while the progressive phase separation for QPSK is 90^o, this scheme nonetheless contains pairs of states with an absolute separation of 180^o, and so a further offset variant of QPSK ensures that transition pathways are in fact limited to a 90^o change (see Fig. 1 for QPSK constellation diagram and phase relationships). Another variant that addresses the dynamic range fluctuation issue is that of $\pi/4$-QPSK, for which the 180^o phase transitions of QPSK are reduced to a maximum of 135^o but with the added advantage of a composite carrier signal (consisting of two constituent signals separated in phase by $\pi/4$) that maintains a constant signal envelope. The above combined advantages of PSK variants has lead to their adoption within various versions of Bluetooth, relatively high-speed wireless LAN, and everyday RFID business transactions as previously identified.

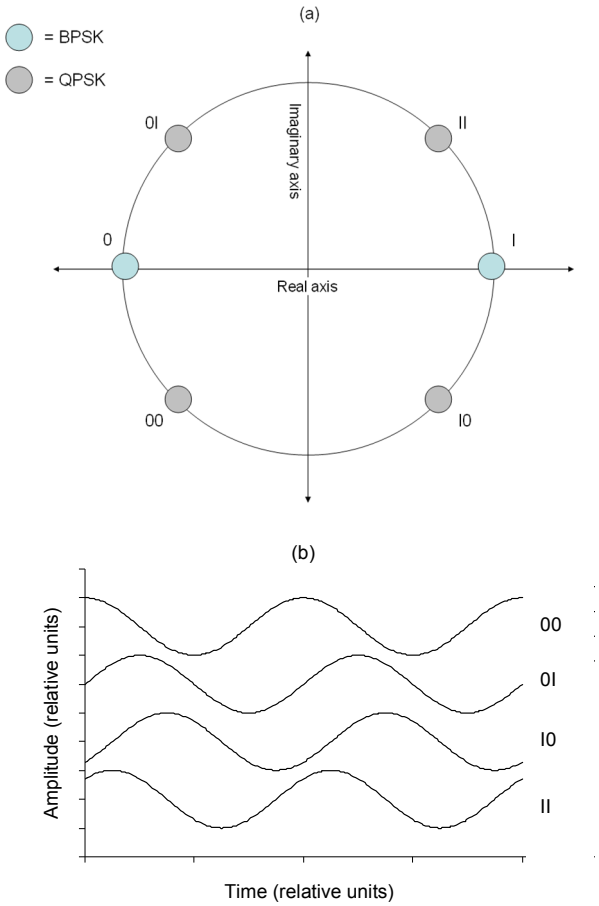

Fig. 1. (a) Constellation diagram for 2-bit QPSK (with 1-bit BPSK included for comparison), and (b) standard graphical phase relationships between RF transmissions for QPSK (amplitudes stacked for comparison purposes).

B. Oscillator Phase Noise

Electrical oscillators (e.g., RLC, Colpits, ring) have a wide range of applications within circuits and electronic control systems (e.g., computer timing control) but may suffer from oscillator phase noise. A natural link, that is perhaps self-evident to some, exists between oscillator phase noise and elements of the previously introduced topic of PSK digital modulation, and this drawn link is necessarily explained and expanded upon throughout the paper.

Oscillator phase noise has been studied and modeled in detail for over 20 years [5]-[8]. The review (tutorial form) article by Lee and Hajimiri [7] in particular provides a thorough overview of the phenomenon at hand which is also often colloquially described as, or directly linked to, oscillator timing "jitter". In brief, oscillator phase noise consists of two primary components, namely, continuous and discrete components. Continuous phase noise is associated with random phase fluctuations about a nominal phase value, with such fluctuations commonly observed and modeled as white and $1/f$ noise [5], [7]. The result of such fluctuations is that the ideal output spectral line of the oscillator is broadened, with a distribution that is also commonly $1/f$ in nature.

Discrete phase noise on the other hand appears as symmetrical side-lobes about the ideal output spectral line of the oscillator [6], [7], with the side-lobes presenting as single- or multi-paired (with an even spacing between pairs), and this discrete component is also commonly referred to as *spurious* phase noise. This alternative terminology is perhaps misleading since it does not serve as true testament to the non-trivial nature of (time dependent) discrete oscillator phase noise as modeled by [7]. For example, a "faulty system connection" may be found within offered simple diagnoses for the presence of spurious phase noise and, while such a single input impulse and time invariant noise mechanisms of older theories can certainly source such noise, more comprehensive time-varying circuit-to-phase noise evolutionary mechanisms, that can for example depend upon the topologies and even amplitude restoring mechanisms of practical oscillators, are truer representations of the underlying model/process complexity. Indeed, communication systems with narrow channel spacings are often constrained by the broadening brought about by phase noise [7], the removal of which can be most challenging and often more difficult than just the simple restoration of a faulty connection.

An example from Simeoni [9] of a typical discrete oscillator phase noise effect is given in Fig. 2, which displays the audiometric output frequency response of a popular brand digital hearing aid following exposure to a 6000 Hz pure tone (approximately symmetrical twin side-lobes about the main 6000 Hz peak are located near 6000 ± 75 Hz as detected by a tympanic microphone in a simulated *in situ* arrangement).

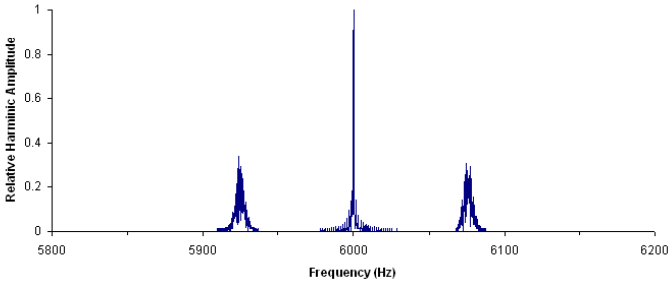

Fig. 2. Example of discrete oscillator phase noise within the output of a popular brand digital hearing aid following exposure to a 6000 Hz pure tone [9] (due to continual technological development, the exemplified digital hearing will not be representative of new, mid-to-high-end digital hearing aids).

C. Study Aims

The primary aim of the present study is to theoretically describe, model and simulate a discrete oscillator phase noise-type effect within a sinusoidal carrier signal and then to present a theoretical formalism that deliberately implements the effect within a new PSK approach. Within the scope of this primary aim, potential practical applications and advantages of such deliberately introduced and controlled signal "artifacts" (here double quotation marks signify the known fact that spectral broadening due to some dynamical signal change is ordinarily considered an undesirable attribute) will be highlighted for the RF communications industry (e.g., in relation to a proposed alternative to Bluetooth-type information exchange).

II. THEORETICAL BACKGROUND

A. Discrete Oscillator Phase Noise-Type Effect Incorporated into a PSK Approach

In accordance with fundamental Fourier analysis and the constituent harmonics of a compound signal within that form of analysis, the n-th harmonic, $X_n(c_n, \omega_n, \phi_n)$, is described as a sine function of angular frequency, ω_n, amplitude, c_n, and phase, ϕ_n. Alternatively, $X_n(c_n, \omega_n, \phi_n)$ may be described as the sum of a cosine function of amplitude, a_n, and a sine function of amplitude, b_n, both with zero phase:

$$X_n(c_n, \omega_n, \phi_n) = c_n \sin(\omega_n t + \phi_n) = a_n \cos(\omega_n t) + b_n \sin(\omega_n t), \quad (1)$$

where $c_n = \sqrt{a_n^2 + b_n^2}$, $\phi_n = \tan^{-1}(b_n / a_n)$, and t is time.

A pure sinusoidal signal within RF communications naturally possesses only one such constituent harmonic in the absence of any deliberate (or indeed unintentional) modulation. The incorporation by the present study of a discrete, time dependent oscillator phase noise-type effect within a PSK-based approach to RF modulation is referred to as discrete spectral PSK (DSPSK) from this point forward. This new DSPSK approach incorporates the said discrete phase noise effect via the additional inclusion of a smooth (e.g., sinusoidal) oscillation of ϕ_n within (1) to give:

$$X_n(c, \omega_n, \omega_\phi, \Delta\phi_n) = c_n \sin(\omega_n t + \Delta\phi_n (\sin(\omega_\phi t) + 1) / 2), \quad (2)$$

where ω_ϕ is the phase modulation frequency and $\Delta\phi_n$ is the phase modulation amplitude for the case of a sinusoidal modulation between 0 and ϕ_n (see Fig. 3).

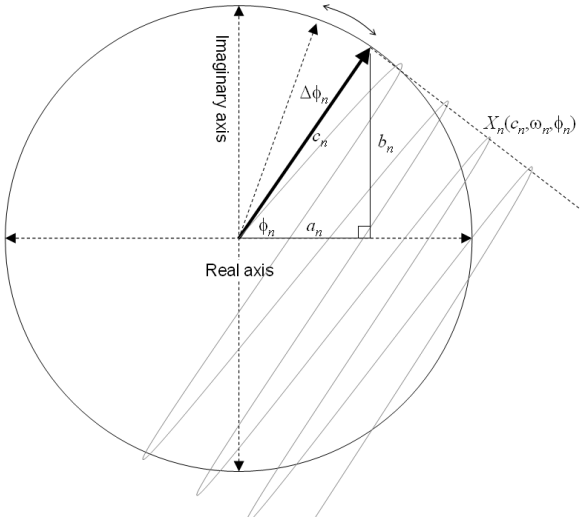

Fig. 3. Diagrammatic representation of a Fourier harmonic with oscillating phase as per (2).

A phase oscillation as indicated above gives rise to discrete, evenly-spaced side-lobe pairs that are symmetrical about the ideal line profile in the frequency domain. The magnitudes of, and hence number of appreciable, off-centre side-lobe pairs formed is a function of the manner and magnitude of the phase oscillation (though lobe formation is independent of the *initial* ϕ_n for a sinusoidal oscillation). Theoretical determination of side-lobe magnitude is achieved by considering side-lobe pairs at angular frequencies given by $\omega_{n,m} = \omega_n \pm m\omega_\phi$, where $m = 1, 2 \ldots\ldots m_{max}$ is side-lobe pair number that monotonically increases away from the primary line profile for a theoretical maximum number of $m_{max} = \omega_n/\omega_\phi$ and $m = 0$ sees reduction to the primary, rather than side, line/lobe profile such that $\omega_{n,m} = \omega_n$ (note that in practice $m_{max} \approx 4$ for side-lobes of appreciable magnitude). The Fourier amplitudes, $c_{n,m} = \sqrt{a_{n,m}^2 + b_{n,m}^2}$, for a side-lobe pair (and the primary centre line) can then be determined by the substitution of (2) into standard Fourier analysis formalism to give:

$$a_{n,m} = \frac{2}{T}\int_0^T c_n \sin(\omega_n t + \Delta\phi_n (\sin(\omega_\phi t) + 1)/2) \cdot \cos(\omega_{n,m} t)\, dt,$$

and (3)

$$b_{n,m} = \frac{2}{T}\int_0^T c_n \sin(\omega_n t + \Delta\phi_n (\sin(\omega_\phi t) + 1)/2) \cdot \sin(\omega_{n.m} t)\, dt,$$

where T is the time duration of the transmitted/received wave packet. Equation (3) differs from the discrete time dependent oscillator phase noise model of Lee and Hajimiri [7] which is naturally based on oscillator modeling approximations, with (3) allowing for more precise lobe calculation because of the absence of any such approximations (i.e., the present approach, based upon exact waveform synthesis, is not subject to any modeling constraints). Note that from this point forward the term lobe refers to side-lobe ($m > 0$) or centre line profile ($m = 0$).

Equation (3) produces unique and discrete lobe combinations with a heavy dependency on $\Delta\phi_n$. As such, each discrete combination may be assigned a unique digital state. Additionally, identification of each state at demodulation may be achieved via a self-referencing approach (i.e., lobe relative magnitude comparison) that offers robustness towards several forms of erroneous signal fluctuation (see Discussion Section).

B. Parallel Binary Number Transmission Through DSPSK

A variant of assigning a digital state to a given discrete lobe combination is to control the discrete lobes such that they physically form a binary number (e.g., where an 8-bit binary number would be formed by eight equally spaced discrete lobes that are either activated or deactivated to "spell-out" the 8-bits in parallel). One means (there are several) of achieving such parallel control is to stack a waveform of the type given by (2) with multiple, evenly-spaced phase modulations, each adopting a (consistent) $\Delta\phi_n$ that is known to produce a single $m = 1$ side-lobe pair alongside the (consistent) primary line profile (i.e., the composite waveform would contain a unique

ω_ϕ for each bit to generate a sole side-lobe to spectrally represent and distinguish that bit):

$$X_n(c, \omega_n, \omega_\phi, \Delta\phi_n) = \sum_{b=1}^{B} p_b c_n \sin(\omega_n t + \Delta\phi(\sin(b\omega_\phi t) + 1)/2), \quad (4a)$$

where the parity operator $p_b = 0$ or 1 offers binary control over the activation of an $m = 1$ side-lobe at a frequency of $\omega_n \pm b\omega_\phi$, and the index b aligns with a particular bit (e.g., $b = 1$ for the most significant bit, $b = B$ for the least significant bit) for a B-bit binary number. Due to the stacking effect of the primary carrier frequency in (4a), the corresponding frequency spectrum can be dominated by a relatively large primary line profile (expected for example when $p_b = 1$ for all or most b) and, as such, (4a) may be additionally mathematically manipulated via the incorporation of primary line nullifying (subtraction) parameters:

$$X_n(c, \omega_n, \omega_\phi, \Delta\phi_n) = \sum_{b=1}^{B}\left[p_b c_n \sin(\omega_n t + \Delta\phi(\sin(b\omega_\phi t) + 1)/2)\right], \\ - Sc_n \sin(\omega_n t + \alpha) \quad (4b)$$

where the scaling factor $S = S(P)$ is a function of P = number of active bits (switched-on parity states), and α is a phase off-set for the subtracted waveform.

III. Method

A. DSPSK

A National Instruments (NI) Labview 2013 (full development system) program was developed to simulate a waveform based on (2) for user-entered ω_n, ω_ϕ, $\Delta\phi_n$ and c_n, with the program subsequently applying standard digital signal processing functions to display the waveform's frequency and power spectra about the primary line profile (i.e., side-lobe region) as consistent with the above Theory Section.

For the purpose of demonstrating typical discrete lobe combinations across $\omega_{n,m}$ as a function of $\Delta\phi_n$ for set ω_n and ω_ϕ, the following input parameter settings were initially applied to (2): $\omega_n/2\pi = 6000$ Hz, $\omega_\phi/2\pi = 10$ Hz, $\Delta\phi_n = 0$ to 2.5π (continuously adjusted), $c_n = 1$. The subsequent simulated waveforms were generated with a time increment of $\Delta t = 50$ μs and $T = 5$ s (i.e., an artificial sampling frequency of $f_s = 20$ kHz and bandwidth of $BW = 10$ kHz were employed). Here, the arbitrary use of a non-RF waveform is representative of the present research's origin stemming from an investigation into an oscillator phase noise side-lobe effect detected within the output for some digital hearing aid amplifiers for an audible pure input tone at 6000 Hz [9]. Any such non-RF computation is directly rescalable and transferable to other base frequencies such as RF, as will be applied and discussed within later Sections.

For each $\Delta\phi_n$ value that produced a discrete lobe (including $m = 0$) combination that was considered desirable (i.e., possessed attributes which readily allowed for relative size comparison/differentiation between lobes for the initially chosen simple range of $m = 0$ to 2, and provided a well-shared distribution of signal power between the lobes of interest), the $\Delta\phi_n$ was recorded and assigned to one of eight 3-bit digital states. The procedure was also repeated whilst adjusting $\omega_\phi/2\pi$ from 1 to 10 Hz, and T from 0.2 to 5 s, so as to determine the combinations of these input parameters associated with the limit of ω_ϕ resolution that was able to maintain the level of lobe discernment achieved by the previously defined initial primary input parameters.

B. Parallel Binary Number Transmission Through DSPSK

For the same initial primary waveform input parameters above ($\omega_n/2\pi = 6000$ Hz, $\omega_\phi/2\pi = 10$ Hz, $c_n = 1$), $\Delta\phi_n$ in (4b) was set to a single side-lobe-producing (at $m = 1$) value of $\Delta\phi_n = 0.75\pi$, with primary line nullifying parameters set to $S = 2/3P$ and $\alpha = 0.35\pi$ (empirically-determined). The Fourier spectrum of the theoretically transmitted waveform was then inspected so as to identify the parallel 8-bit ($B = 8$) binary number representation as expected from (4b) for the following binary and parity input settings:

$P = 8$, p_1 to $p_8 = 1$ ($\equiv$ 11111111)

$P = 6$, $p_1, p_2, p_3, p_5, p_6, p_8 = 1, p_4, p_7 = 0$ ($\equiv$11101101)

$P = 5$, $p_1, p_3, p_4, p_7, p_8 = 1, p_2, p_5, p_6 = 0$ ($\equiv$ 10110011).

IV. Results

A. DSPSK

Table 1 presents the $\Delta\phi_n$ values, together with their assigned 3-bit digital states, for the primary test waveform as specified by (2) with input parameters of $\omega_n/2\pi = 6000$ Hz, $\omega_\phi/2\pi = 10$ Hz and $c_n = 1$. Each Table 1 entry also includes the corresponding logical discernment mechanism used within the aforementioned relative self-referencing approach, with A, B and C corresponding to the relative amplitudes of $m = 0$, 1, and 2 lobes respectively.

TABLE I. Phase modulation amplitude, $\Delta\phi_n$, with corresponding assigned 3-bit digital state and logical discernment mechanism (with A, B and C corresponding to the relative amplitudes of $m = 0$, 1, and 2 lobes respectively), for the primary test waveform as specified by (2) with input parameters of $\omega_n/2\pi = 6000$ Hz, $\omega_\phi/2\pi = 10$ Hz and $c_n = 1$.

3-bit DSPSK Scheme Elements		
$\Delta\phi_n$ ($\times\pi$ radians)	***3-bit digital state***	***Lobe-based logical discernment***
0	000	A > (B = C = 0)
0.75	001	A > B > C
2.50	010	(D >) A > C > B[a]
1.00	011	B > A > C
1.44	100	B > C > A
2.25	101	C > A > B
1.80	110	C > B > A
1.59	111	A = 0 (< D) < B = C[a]

[a] The m = 3 lobe (≡ D nomenclature) may be optionally included to enhance state discernment.

Fig. 4 displays the primary test waveform's frequency (lobe) spectrum for each identified $\Delta\phi_n$, along with A, B and C lobe annotations, in accordance with Table 1. A straight forward means of extending Table 1 to form a 4-bit version of a similar approach is outlined within the Discussion Section.

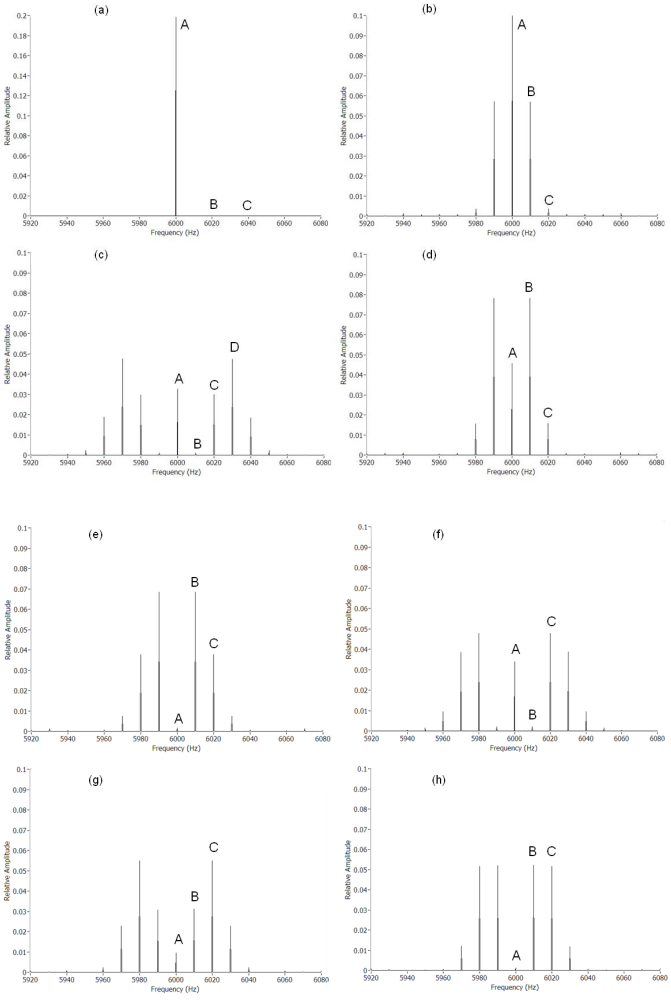

Fig. 4. Primary test waveform's frequency (lobe) spectrum for each identified phase amplitude modulation $\Delta\phi_n$ value of Table 1, (a) 0, (b) 0.75π, (c) 2.50π, (d) 1.00π, (e) 1.44π, (f) 2.25π, (g) 1.80π and (h) 1.59π radians (remaining input parameters same as for Table 1).

For the example phase oscillation amplitude of $\Delta\phi_n = 2\pi$, Fig. 5 displays the dependency of lobe resolution and bandwidth on ω_ϕ and T by comparing the default (sharp) resolution case of $\omega_\phi = 10$ Hz, $T = 5.0$ s (Fig. 5a) with the spectral resolution limiting variants of $\omega_\phi/2\pi = 10$ Hz, $T = 0.4$ s (Fig. 5b), $\omega_\phi/2\pi = 5$ Hz, $T = 0.8$ s (Fig. 5c), and $\omega_\phi/2\pi = 2$ Hz, $T = 1.0$ s (Fig. 5d), with subsequent spectral resolution limits summarized within Table 2. Lobe bandwidth, *LBW*, in Table 2 is given by $8 \times \omega_\phi$, based on previously indicated in-practice significant m values.

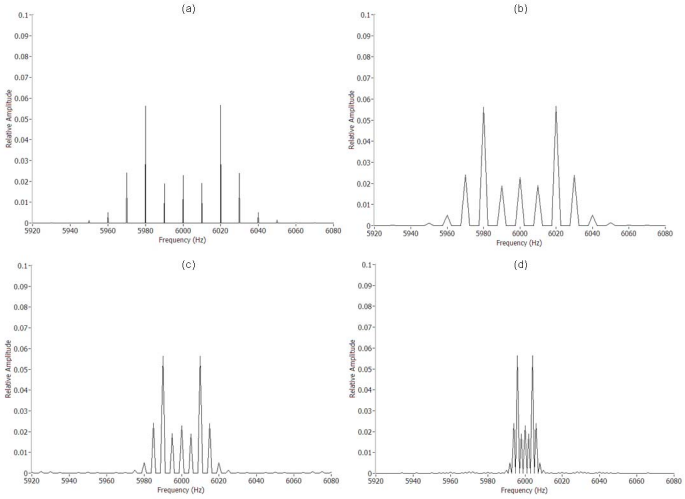

Fig. 5. Lobe resolution and bandwidth for a phase oscillation amplitude of $\Delta\phi_n = 2\pi$ as a function of phase oscillation frequency, ω_ϕ, and waveform duration, T. (a) $\omega_\phi/2\pi = 10$ Hz, $T = 5.0$ s, (b) $\omega_\phi/2\pi = 10$ Hz, $T = 0.4$ s, (c) $\omega_\phi/2\pi = 5$ Hz, $T = 0.8$ s and (d) $\omega_\phi/2\pi = 2$ Hz, $T = 1.0$ s (remaining input parameters same as for Table 1).

TABLE II. LIMITING COMBINATIONS OF PHASE MODULATION FREQUENCY, ω_ϕ, LOBE BANDWIDTH, *LBW*, AND SAMPLE PERIOD, T, THAT MAINTAIN RESOLVABLE LOBES FOR THE EXAMPLE CASE OF $\Delta\phi_n = 2\pi$, $\omega_n/2\pi = 6000$ HZ.

Parameter Combinations Allowing Lobe Resolution		
$\omega_\phi/2\pi$ ***(Hz)***	***LBW*** ***(Hz)***	***T*** ***(s)***
2.0	16	1.0
5.0	40	0.8
10.0	80	0.4

From the expected linear relationship between ω_ϕ and T that is verified by Table 2, the limiting value of T required to achieve spectral lobe resolution for a given ω_ϕ is given by $T_{\lim} = -7.55\times10^{-2}\,\omega_\phi / 2\pi + 1.16$. For a generic ω_n, the above limiting condition result is more generally written as:

$$T_{\lim} = (-453\omega_\phi + 4.37\times10^4) / \omega_n . \quad (5)$$

From (5), Table 2 results are transferable to the RF case of $\omega_n/2\pi = 2.4$ GHz, as per Table 3, from which RF bit transmission rates are readily calculated.

TABLE III. LIMITING COMBINATIONS OF PHASE MODULATION FREQUENCY, ω_ϕ, LOBE BANDWIDTH, *LBW*, AND SAMPLE PERIOD, *T*, THAT MAINTAIN RESOLVABLE LOBES FOR THE EXAMPLE CASE OF $\Delta\phi_n = 2\pi$, $\omega_n/2\pi = 2.4$ GHz.

Parameter Combinations Allowing Lobe Resolution		
$\omega_\phi/2\pi$ ***(MHz)***	***LBW*** ***(MHz)***	***T*** ***(μs)***
0.125	1.0	2.9
0.8	6.4	2.5
2.0	16	2.0
4.0	32	1.0

Based on Table 3, the postulated 3-bit version of the presented technique theoretically allows for a RF ($\omega_n/2\pi = 2.4$ GHz) transmission rate of 1 to 3 Mbit/s for *LBW* = 1.0 to 32 MHz respectively. For a 4-bit version (see Discussion Section), this transmission rate increases to 1.4 to 4 Mbit/s for the same tabulated *LBW* values.

B. Parallel Binary Number Transmission Through DSPSK

Figs. 6a to 6c respectively represent the frequency domain representation of the example 8-bit binary numbers 11111111 ($P = 8$), 11101101 ($P = 6$), and 10110011 ($P = 5$), as modeled and theoretically transmitted by (4b) for input parameters of $\omega_n/2\pi = 6000$ Hz, $\omega_\phi/2\pi = 10$ Hz, $c_n = 1$, and $\Delta\phi_n = 0.75\pi$ (generates a dominant $m = 1$ side-lobe), and primary line nullifying input parameters (respective scaling and phase off-set parameters) of S=2/3P and $\alpha = 0.35\pi$.

In accordance with Table 3, the theoretical data transmission rate for the above 8-bit parallel binary number transmission is 3 to 8 Mbit/s, but for a doubling of the *LBW* that would otherwise be expected from Table 3, i.e., *LBW* = 2.0 to 64 MHz respectively for these 8-bit transmission rates (since the effective m_{max} is inherently increased from 4 to 8). A theoretical variation to this parallel approach, with a means of further extending the data transmission rate, is deliberated within the Discussion Section to follow.

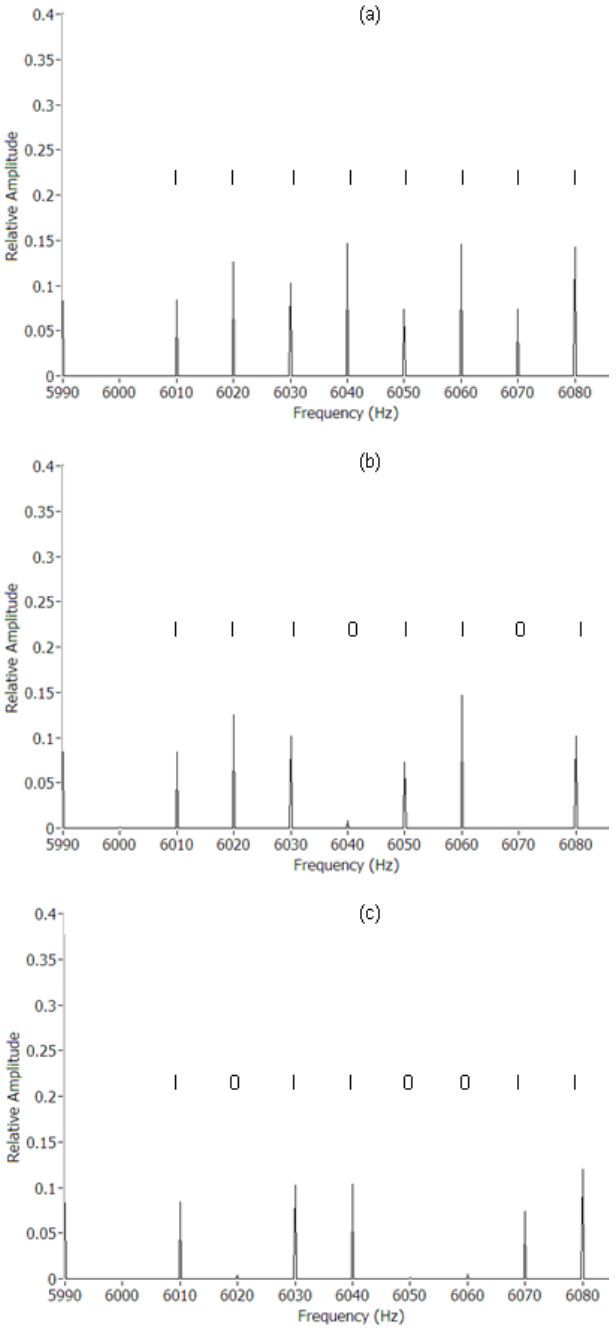

Fig. 6. Frequency spectrum of example 8-bit binary numbers (a) 11111111 ($P = 8$), (b) 11101101 ($P = 6$), and (c) 10110011 ($P = 5$) as modeled and theoretically transmitted by (4b) for input parameters of $\omega_n/2\pi = 6000$ Hz, $\omega_\phi/2\pi = 10$ Hz, $c_n = 1$, $\Delta\phi_n = 0.75\pi$, S=2/3P and $\alpha = 0.35\pi$, where P is the number of active bits.

V. DISCUSSION

A. DSPSK

The presented DSPSK technique uniquely applies a simple analog-type modulation to achieve a digital-type demodulation, with the lobe-based symbol-set to which the DSPSK demodulator maps also being unique (though the applied principle of symbol-set mapping is generically standard for PSK). These unique attributes result in several ensuring technique advantages. The first of these advantages is revealed by appreciation of the fact that other PSK schemes require a uniform angular spacing in phase about the schemes' constellation diagrams so as to maximize the separation and distinguishability of states. This fact is particularly evident within the 8-PSK scheme (a 3-bit scheme with eight evenly-spaced digital states about the scheme's constellation diagram) which is not widely employed because of its known signal error rate associated with tight state spacing. However, unique to DSPSK is the fact that the relevant modulation parameter of $\Delta\phi_n$ can be unevenly separated and small changes in $\Delta\phi_n$ can result in discretely different digital modulation outcomes to readily allow for discernment between digital states (for a constant ω_ϕ).

Another DSPSK advantage stems from the inherently smooth sinusoidal oscillation of ϕ_n and subsequent smooth transition between digital states of the proposed technique (in contrast conventional PSK schemes utilize abrupt ϕ_n transitions). Thus, *extra* unwanted spectral broadening that often results from the abrupt between-state transitions of conventional schemes will be avoided for the proposed technique (Gaussian frequency-shift keying or GFSK is for example a popular modulation process that involves signal smoothing with a Gaussian filter for the specified reason, and which would not be required for DSPSK).

As already outlined within the Introduction Section, self-referencing modulation techniques generally offer some advantage in relation to reducing deleterious effects of dynamic range fluctuation and simplifying demodulation processing/instrumentation due to not requiring a comparison source. DSPSK self-referencing similarly but also uniquely, via relative lobe magnitude comparison for logic state discernment, offers advantage in the form of potential robustness against broad spectrum noise (the most common form of noise affecting RF communications) since the lobes are fixed and coupled in regards to their relative magnitudes, and are affected by such broad spectrum noise to the same approximate degree. The signal amplitude fluctuation immunity offered by the technique is further enhanced by the fact that side-lobes are produced as symmetrical pairs, thus offering noise reduction via symmetrical averaging which inherently reduces noise by a factor of $\sqrt{2}$.

While a RF transmission comparable to a *single-source* transmission based upon (2) can be achieved via parallel multi-frequency transmission without phase modulation (i.e., one transmitter for each lobe frequency), such a "transmission-equivalent" approach loses the DSPSK technique's identified advantages.

With the above DSPSK advantages also comes identified acceptable transmission rates of up to 3 Mbit/s for the demonstrated 3-bit scheme, rates that are comparable to other PSK techniques and indeed Bluetooth 2.0 which also enables a rate of 3 Mbit/s. It should be noted that for the presented DSPSK approaches, transmission rates are based on T_{lim} values as required to achieve resolution following theoretical sampling and Fourier analysis. The use of multi-receivers (one for each lobe) or an analog frequency analyzer-based receiver could conceivably increase these determined transmission rates. Note also that transition rates and *LBW*s for RFID frequencies other than the targeted 2.4 GHz case may be routinely generated via application of (5).

A natural disadvantage of the presented DSPSK technique is the fact that power is ultimately distributed (and thus dissipated) across several lobes and thus across a frequency band, albeit narrow. This disadvantage may decrease the effective transmission range (when comparing with other techniques for the same RF power emission), in turn perhaps lending the technique to shorter-range RFID applications. However, any power per lobe lowering (if comparing to a single line profile transmission) is offset by the previously discussed amplitude fluctuation immunity. An additional associated disadvantage is the inherent effective doubling of bandwidth due to the generation of symmetrical side-lobe pairs, but again stated *LBW* values are within comparable and practically acceptable ranges.

The simple manner of logic state discernment presented by the 3-bit case of Table 1 represents just one of many permutations of discrete lobe configuration arrangement, and indeed lobes associated with $m = 0$ to 2 can be logically combined to form sixteen (4-bit) states by incorporating a secondary level of assignment. For example,
$1000 \equiv A = B < C$,
$1001 \equiv A = C > (B = 0)$,
$1010 \equiv A = B > C$,
$1011 \equiv A = C < B = 0$, etc…, for which $\Delta\phi_n$ can be respectively identified as 1.95π, 2.42π, 0.855π and 1.135π.

Other permutation examples may include expanded use of the $m = 3$ (D) lobe. Indeed, when the simple primary level state assignment method as per Table 1 is applied to the $m = 0$ to 3 case, the technique's potential is revealed further by the fact that the Table 1 primary level approach then offers a minimum of 4! logical states (e.g., A > B > C > D, A > C > B > D, etc…) before secondary level lobe combinations are considered. The 4! number of states in that case clearly compares favorably to the standard 2^4 number of states associated with a conventional 4-bit binary number system. However, to access all such 4! states greater lobe control is required, achieved for example by the superposition of two (2)-type waveforms with independent $\Delta\phi_n$ and c_n control for the same ω_n and ω_ϕ, as per (6) below where the independent control is represented by subscripts 1 and 2 placed upon some n:

$$X_n(c,\omega_n,\omega_\phi,\Delta\phi_n) = c_{n_1}\sin(\omega_n t + \Delta\phi_{n_1}(\sin(\omega_\phi t)+1)/2) + c_{n_2}\sin(\omega_n t + \Delta\phi_{n_2}(\sin(\omega_\phi t)+1)/2). \quad (6)$$

B. Parallel Binary Number Transmission Through DSPSK

The theoretical transmission rate of up to 8 Mbit/s for 8-bit parallel binary number transmission achieved through stacked phase modulation as per (4b) and as demonstrated by Figs. 6a to 6c, exceeds the transmission rates of several other PSK techniques, but again with the disadvantage of a comparatively widened bandwidth. This approach offers a conventional number of states (e.g., eight lobes or bits offer 2^8 digital states) in accordance with the fact that (4b) allows for switching one or more of the eight lobes off or on with approximate constant lobe amplitude. However, if one were to introduce lobe amplitude control (e.g., via c_n becoming $c_{n,b}$ in (4b)), then the potential for a $B!$ number of states (as per the previously applied primary level logic state assignment method of Table 1) rather than a traditional 2^B number of states is again revealed, offering theoretical transmission rates of up to 15 Mbit/s (which could be increased further via the superposition of states or the introduction of secondary levels of state assignment as previously discussed).

C. Future Applications within RF Communications

Given the highlighted theoretical advantages of the presented RF *modulation* → *transmission* → *demodulation* techniques involving phase oscillation control, DSPSK variants offer potential alternatives to the several other forms of compound RF communication/modulation methods applied within industry (e.g., Bluetooth, DAB+) that provide enhanced security and interference resistance. High-speed primary carrier frequency hopping spread spectrum (FHSS) transmission techniques (e.g., utilized by Bluetooth in the range 2.400 to 2.484 GHz, and by other non-Bluetooth commercial wireless transmitter/receiver devices such as the Audiomate AM8112 used for personal audio communication), could also obviously be added to further enhance the presented DSPSK variants (e.g., enhancement in terms of security and interference resistance). In fact, a form of FHSS may be easily incorporated within DSPSK since the phase modulation frequency (which sets the spacing between lobes) can be deliberately and easily "hopped" during transmission to vary the tuning of the lobes. As an example of the inherent ease of a FHSS-style implementation, a relevant modulation parameter was set to $\omega_\phi/2\pi = 10$ Hz for most simulations of this study, however, within Fig. 5 $\omega_\phi/2\pi$ was varied from 2 to 10 Hz to vary the tuning of, and thereby inadvertently hopping, the lobes. Thus, in summary DSPSK approaches possess generic commercial application potential in the same way that Bluetooth and other known RF modulation schemes have been commercially applied within industry and society.

More specifically, DSPSK would be particularly suited to RFID applications that require a moderate-to-high transmission speed, stability, and reliability over a relatively short transmission range (as justified by previous advantage discussions for this Section), in conjunction with enhanced security (e.g., the exceptionally high level of wireless security for smart payments, banking, restricted access control, etc.). This proposed commercial application aspect is aided by the DSPSK demodulator mapping approach which is both highly specific and arbitrary. The arbitrary nature is demonstrated by the fact that the state assignment method of Table 1 is just one of many possible permutation or code examples that could be similarly applied. Thus, cryptography enhancement is achievable by the controlled hopping between such codes which would be difficult to decipher upon any malicious or other interception (much more so than for conventional PSK schemes with their simple ciphers).

D. Practical Considerations and Future Verification Testing

The predicated theoretical data transfer rates require practical verification in the future. This point is especially the case since in essence data lobes are generated by a relatively low frequency modulation placed upon a much higher carrier frequency, and so modulation is subtle over a limited number carrier frequency cycles, which is not the case for BPSK and similar origin PSK techniques that are based on an abrupt change in carrier frequency phase. However, confidence in the future viability/verification of the stated theoretical DSPSK data transfer rates can be gained from the earlier discussion point that the DSPSK effect can be mirrored by parallel frequency transmission (i.e., "'broadband"), which is of course proven and made possible by the use of advanced transmitter/receiver circuitry as similarly required by DSPSK.

E. Quantum Computing Applications

A perhaps not so obvious point of interest for the DSPSK approaches stems from the fact that an analogous association can be drawn between the analyzed off-centre lobes of DSPSK and the off-centre wave function and reaction cross-section spectral resonances [10] observed in some (wave-like) quantum mechanically described systems that involve inherently complex oscillatory system modulations. Moreover, the future control of such (energy specific) wave (probability density) function resonances, particularly in simple systems of low mass and particle number, may lead to a potential DSPSK application within quantum computing, since the DSPSK-like control and utilization of wave function resonances may provide a means of discrete digital information storage, display and manipulation.

The analogy between DSPSK and probabilistic, parallel quantum computing is further revealed by appreciation of the fact that B quantum bits (qubits) can simultaneously represent an arbitrary superposition of up to 2^B states (or effectively perform 2^B calculations at once) rather than represent just one of 2^B states at a given time which of course represents the confines of conventional binary bit-based computing [11]. Similarly, presented DSPSK techniques utilize the superposition of states to give rise to parallel binary information identification and a number of represented states (e.g., $\geq B!$) that far exceeds that of the conventional 2^B. This possible application represents an exciting potential future construct; the hypothetical and ambitious nature of the construct should not be a deterrent to further investigation, given that even today many current elements of quantum computing are seen as theoretical, with the likelihood of quantum computers replacing (and even outperforming for every-day computations) conventional desktop computer technology being a continuing topic of contentious debate.

VI. Conclusion

For the demonstrated discrete spectral phase-shift keying (DSPSK) RF *modulation* → *transmission* → *demodulation* techniques involving smooth phase oscillation control and subsequent control of discrete off-centre side-lobes about the primary line profile of the carrier spectrum, the following findings have been concluded:

- The techniques, while relatively rudimentary, are novel in their manner of analog-type modulation leading to a digital-type demodulation.
- The techniques offer competitive data transmission rates (and bandwidths as specified within) of up to 3, 4 and 8 Mbit/s for 3-bit, 4-bit and 8-bit transmission versions respectively.
- Extensions of the presented techniques allow for transmission rate increases. For example, a variant involving the superposition of two waveform oscillations lead to an "exponential" increase in the number of possible outputs (e.g., $B!$ versus the 2^B states of a traditional B-bit binary system) based on a primary level state assignment that was capable of further secondary level extensions.
- The techniques offer the advantage of robustness (in terms of resilience towards interference and distortion), a consequence of amplitude fluctuation immunity, self-referencing, smooth waveform transitions between digital states, and single RF source control.
- An additional advantage worthy of separate mention and related to the above-noted digital state generation efficiency, is that the techniques are distinguished from known PSK techniques by the fact that uneven and small changes in the relevant phase-based modulation parameter can result in highly distinguishable output states.
- The technique offers broad application potential across the RF communications industry (e.g., within a Bluetooth-style approach to data transfer with readily incorporated FHSS), most notably where enhanced transaction security is paramount.
- The practical verification of stated theoretical data transfer rates is required, and is an intended project, for the future.

References

[1] Atmel Corporation. (2005). *Application note: understanding the requirements of ISO/IES 14443 for type B proximity contactless identification cards* [Online]. Available://www.atmel.com/images/doc2056.pdf.

[2] T. S. Rappaport, *Wireless communications principles and practice 2nd ed.* Upper Saddle River, NJ: Prentice Hall PTR, 2009.

[3] B. Sklar, *Digital communications fundamentals and applications 2nd ed.* Harlow, Essex: Pearson, 2014.

[4] W. Stallings, *Wireless communications and networks 2nd ed.* Harlow, Essex: Pearson, 2014.

[5] T. A. D. Riley, M. A. Copeland, T. A. Kwasniewski, Delta-sigma modulation in fractional-*N* frequency synthesis. *IEEE Journal of Solid State Circuits*, *28*, 553-559, 1993.

[6] B. Razavi, A study of phase noise in CMOS oscillators. *IEEE Journal of Solid State Circuits*, *31*, 331-343, 1996.

[7] T. H. Lee, A. Hajimiri, Oscillator phase noise: a tutorial. *IEEE Journal of Solid State Circuits*, *35*, 326-336, 2000.

[8] A. Demir, Computing timing jitter from phase noise spectra for oscillators and phase-locked loops with white and 1/*f*noise. *IEEE Transactions on Circuits and Systems–I: Regular Papers*, *53*, 1869-1884, 2006.

[9] R. J. Simeoni, "Response comparison of digital hearing aids," in *Engineering and Physical Sciences in Medicine Conference: Excellence Through Innovation and Professional Development*, Perth, 3-7 November, 2013, pp. 236.

[10] E. Lavert-Ofir, Y. Shagam, A. B. Henson, S. Gersten, J. Klos, P. S. Zuchowski, J. Narevicius, E. Narevicius, Observation of the isotope effect in sub-kelvin reactions. *Nature Chemistry 6*, 332-335, 2014.

[11] N. S. Yanofsky, M. A. Mannucci, *Quantum computing for compter scientists.* New York, NY: Cambridge University Press, 2008.